

Surface-acoustic-wave-induced carrier transport in quantum wires

F. Alsina,* P. V. Santos, H.-P. Schönherr, W. Seidel, and K. H. Ploog
Paul-Drude-Institut für Festkörperelektronik, Hausvogteiplatz 5–7, 10117 Berlin, Germany

R. Nötzel

Paul-Drude-Institut für Festkörperelektronik, Hausvogteiplatz 5–7, 10117 Berlin, Germany
and COBRA Inter-University Research Institute, Eindhoven University of Technology, 5600 MB Eindhoven, Netherlands

(Received 18 July 2002; published 31 October 2002)

The ambipolar transport of photogenerated electron-hole pairs by surface acoustic waves (SAW's) in coupled GaAs quantum wells (QW's) and quantum wires (QWR's) is investigated by spatially and time-resolved photoluminescence. Experimental configurations for SAW propagation direction parallel or perpendicular to the QWR's have been studied. In the first configuration, the QWR confinement potential inhibits lateral carrier diffusion. The carriers are then efficiently transported along the wire as well-defined charge packages with a repetition rate corresponding to the SAW frequency. In the second configuration, we demonstrate that the SAW can be used to transfer electron-hole pairs generated in the QW into the QWR. We also provide clear evidence for the extraction of carriers from the QWR into the QW, when the SAW piezoelectric field is sufficiently strong to overcome the QWR confinement potential.

DOI: 10.1103/PhysRevB.66.165330

PACS number(s): 78.55.Cr, 77.65.Dq, 77.65.Ly

I. INTRODUCTION

Present semiconductor technologies allow for the combination of different low-dimensional semiconductor structures like quantum wells (QW's), wires (QWR's), and dots (QD's) on the surface of a single semiconductor crystal. The functionality of these structures depends, in most cases, on the ability to transfer charge carriers between them. A typical example is the quantum dot laser.¹ Here charge carriers injected into the continuum of states of a QW have to be efficiently transferred to the localized states of the QD's embedded in the QW. In this framework, the study of the transport dynamics of photogenerated carriers using spectroscopic techniques has become of special interest for both device operation and fundamental physics. As an example, spatially and time-resolved near-field spectroscopy of sidewall QWR's on patterned GaAs (311)A substrates² has led to a detailed comprehension of the carrier transfer between the QWR and the neighboring QW in these nanostructures.^{3,4}

The lateral transfer of electron and hole pairs has until now mainly relied on diffusive transport. Surface acoustic waves (SAW's) provide an additional degree of freedom to control lateral carrier transfer. The type-II potential modulation induced by the piezoelectric field of a SAW in III-V semiconductors is sufficiently strong to ionize photogenerated excitons and to spatially separate and transport the free electrons (e) and holes (h) with the SAW velocity v_{SAW} .⁵ Recently, Bödefeld *et al.*⁶ demonstrated the controlled transfer of photogenerated electron-hole pairs by a SAW between a QW and the QD's embedded in it.

In this paper, we investigate the SAW-induced ambipolar transport of photogenerated carriers between a QW and a QWR by using spatially and time-resolved photoluminescence spectroscopy (PL). The system chosen for investigation consists of sidewall QWR's embedded in a QW, both grown on the (311)A GaAs surface. A particular feature of this coupled system of QW's and QWR's is that the transport depends on whether the SAW propagates parallel or perpen-

dicular to the QWR. In the former case, we demonstrate that carrier diffusion parallel to the wavefront, which characterizes the SAW-induced transport in QW's,⁷ is inhibited by the QWR confinement potential. As a result, the QWR acts as a channel for the ambipolar transport of carriers over distances several orders of magnitudes larger than the QWR width. Time-resolved measurements show that the transport takes place synchronously with the SAW frequency ω_{SAW} . In the perpendicular configuration, the SAW field can be used to transfer carriers from the QW into the QWR. In addition, we give experimental evidence for the extraction of carriers from the QWR into the QW, when the SAW potential Φ_{SAW} is sufficiently large to overcome the QWR confinement potential.

This paper is organized as follows. We start in Sec. II with a description of the sample structures and the experiments. The obtained results are presented in Sec. III, where in the first and second subsections we provide the necessary background about SAW propagation on a (311) GaAs surface and the characteristics of the PL spectra, respectively. The next two subsections are devoted to the SAW-induced transport of photogenerated carriers along the QWR and to QW-QWR coupling, in that order. Spatially and time-resolved PL measurements are discussed in each subsection. Section IV summarizes the main conclusions of this work.

II. EXPERIMENTAL DETAILS

The semiconductor structures used in the present investigations consist of three nominally undoped GaAs QW's separated by 10-nm-thick $\text{Al}_{0.3}\text{Ga}_{0.7}\text{As}$ barriers grown by molecular beam epitaxy (MBE) on patterned GaAs (311)A substrates. Each GaAs QW is 6 nm thick and the first one is located 120 nm below the surface. Prior to the MBE growth, mesa stripes with a height of approximately 20 nm and oriented along the $[0\bar{1}1]$ direction were etched on the surface of the substrate. The formation of a fast-growing sidewall at the edge of the mesa with a convex unafaceted surface profile

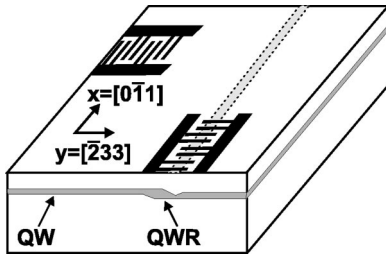


FIG. 1. Structure of sidewall QWR sample on patterned (311)A GaAs substrates with interdigital transducers (IDT's) for the generation of SAW's.

results in a vertical stack of quasiplanar lateral QWR's, which are twice as thick as the QW's and with lateral extension of approximately 50 nm. Further details about the fabrication and electronic properties can be found in Ref. 2. The separation between adjacent wires, which is determined by the original mesa patterning, is 20 μm .

SAW's propagating either parallel or perpendicular to the QWR's on the (311) surface were generated by aluminum split-finger interdigital transducers (IDT's) deposited on the sample surface, as illustrated in Fig. 1. The IDT's were designed for operation at a wavelength λ_{SAW} of 5.6 μm . This corresponds to a frequency $\omega_{\text{SAW}}/(2\pi)$ at 12 K of 533 and 434 MHz for the $[0\bar{1}1]$ and $[\bar{2}33]$ directions, respectively, of the (311) surface. Each split-finger IDT consists of 700 aluminum electrode pairs with an aperture of 120 μm . In the following, we will specify the acoustic power in terms of the nominal radio-frequency (rf) power P_{rf} applied to the IDT's, which does not take into account the coupling losses due to electrical mismatch.

The investigations were conducted by performing spatially and time-resolved PL to dynamically probe the spatial distribution of carriers during transport by a SAW. PL measurements were carried out at 12 K using a microscope with adjustable illumination and detection areas, each with a diameter of about 2 μm . The adjustable separation between the illumination and detection spots allows us to investigate the ambipolar carrier transport within a length scale of a few μm 's.^{7,8} Excitation below the $\text{Al}_{0.3}\text{Ga}_{0.7}\text{As}$ barriers was provided by the continuous radiation from a Ti:sapphire laser ($\lambda_L = 750 \text{ nm}$) or by a pulsed semiconductor laser ($\lambda_L = 687 \text{ nm}$) with a pulse width of 75 ps. The time-averaged PL was detected using a cooled charge-coupled-device detector. For time-resolved measurements, an avalanche photodiode (APD) with time resolution of approximately 0.35 ns was used as detector. In this case, the APD was synchronized with the rf generator employed to drive the IDT's.

III. RESULTS

A. SAW propagation

The experimental configuration in Fig. 1 presupposes that SAW's with longitudinal piezoelectric fields can be generated along the $x=[0\bar{1}1]$ and $y=[\bar{2}33]$ directions of the (311) surface. These directions are not equivalent with respect to the SAW modes.^{9,10} In order to investigate the SAW

TABLE I. Propagation properties of SAW's along the $x=[0\bar{1}1]$ and $y=[\bar{2}33]$ directions of the (311) GaAs surface obtained from rf-transmission and reflection measurements. v_{SAW} is the measured SAW propagation velocity. r_a and r_f denote the measured acoustic power and the calculated peak value of the longitudinal piezoelectric field, respectively, normalized to those for a Rayleigh SAW propagating along the $[011]$ direction of the (100) surface (last row). r_a was determined from the S_{11} rf-reflection coefficient.

Prop. dir./ surface	v_{SAW} (m/s)	r_a	r_f
$[0\bar{1}1]/(311)$	2932	1.0	1.03
$[\bar{2}33]/(311)$	2677	0.42	0.785
$[011]/(100)$	2862	1.0	1.0

propagation properties, identical SAW delay lines were also deposited on plain (311) GaAs as well as on (100) GaAs substrates. The SAW velocities for the different configurations are listed in Table I. These velocities were obtained from measurements of the rf-transmission across the delay lines using a network analyzer. While comparable propagation velocities along $\langle 110 \rangle$ directions are observed for the (100) (denoted as the $[011]/(100)$ mode) and (311) ($[0\bar{1}1]/(311)$ mode) surfaces, the velocity along the $[\bar{2}33]$ axis of the (311) surface ($[\bar{2}33]/(311)$ mode) is considerably lower. The third column of the table shows the effective coupling coefficient r_a relative to that of the $[011]/(100)$ mode. r_a specifies the fraction of the applied r_f power that is coupled into the acoustic mode (equal IDT's were employed for the different SAW propagation directions). r_a was determined from the dip in the S_{11} rf-reflection coefficient of the IDT's at the SAW resonance frequency. As for the propagation velocity, r_a is also considerably smaller for the $[\bar{2}33]/(311)$ mode.

Further information about the SAW properties were obtained from numerical calculations of the SAW fields. The latter show that while the $[\bar{2}33]/(311)$ and $[011]/(100)$ modes are strongly localized on the sample surface, the $[0\bar{1}1]/(311)$ one is a leaky mode (or pseudosurface wave) with a low attenuation coefficient.¹⁰ The ratio between the r_a for the $[\bar{2}33]/(311)$ and $[0\bar{1}1]/(311)$ of 0.42 compares reasonably well with the calculated value of 0.53 reported in Ref. 10. The last column in Table I shows the amplitude of the SAW piezoelectric field r_f calculated for a constant SAW acoustic power density. r_f is also lower for SAW's along the y direction of the (311) surface. The longitudinal piezoelectric field F_y for the $[\bar{2}33]/(311)$ mode is by a factor $r_f\sqrt{r_a} \sim 0.51$ smaller than in the other cases.

B. Photoluminescence spectra

Figures 2(a) and 2(b) display typical PL spectra recorded from the QWR and from the adjacent QW, respectively. The precise location of the QWR was found by adjusting the exciting laser spot laterally across the mesa edge in order to

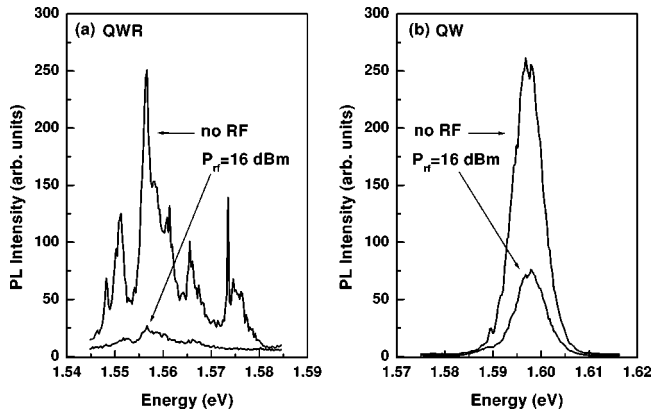


FIG. 2. Photoluminescence spectra recorded in the (a) QWR and (b) QW regions in the absence and in the presence of a SAW.

maximize the QWR PL signal. The emission intensity from the QW has a minimum at this position.

The QWR emission band consists of several sharp peaks separated by a few meV and superimposed on a smooth background. With increasing light intensity, these sharp peaks evolve into a broadened single emission band. The average energy of the emission band changes by as much as 10–15 meV when the laser spot is moved along the QWR axis. These features are attributed to inhomogeneities in the QWR, which lead to potential fluctuations.^{11,12} Emission from localized excitons in wirelike boxes with different lengths in addition to thickness fluctuations account for most of the characteristics of the PL spectrum. The energy variation given by those potential fluctuations is, however, well

below the mean value of the QWR lateral confinement potential of about 40 meV, as determined from the energy separation between the PL emission bands in Figs. 2(a) and 2(b).

Under the influence of a SAW, the PL intensity from both the QWR [Fig. 2(a)] and QW [Fig. 2(b)] becomes strongly suppressed as a consequence of (i) the ionization of the photoexcited excitons^{5,13,14} and of (ii) the sweep of the electron-hole pairs out of the microscopic PL detection spot by the longitudinal component of the piezoelectric field, which moves with the SAW propagation velocity v_{SAW} .^{14,15} The latter will be investigated in detail in the remainder of this section. We note that the degree of PL quenching also depends on the excitation intensity due to the partial screening of the piezoelectric field by photogenerated carriers.¹⁴

C. SAW-induced transport along the QWR's

1. Spatial profiles

The SAW-induced ambipolar transport of photogenerated carriers in (311) QW's was investigated by measuring the spatial distribution of the PL excited by a microscopic laser spot.^{7,8} In these measurements, the generation spot G was placed in the SAW propagation path some micrometers away from a semitransparent metal stripe deposited on the sample surface, as illustrated in Fig. 3(a). The metal stripe short-circuits the SAW piezoelectric field and thus forces the carriers transported by the SAW to recombine.⁵

The contour plots in Figs. 3(b) and 3(c) show the spatial dependence of the integrated PL intensity in the absence and in the presence of a SAW, respectively, obtained when G is placed in the QW region and away from the QWR. In the

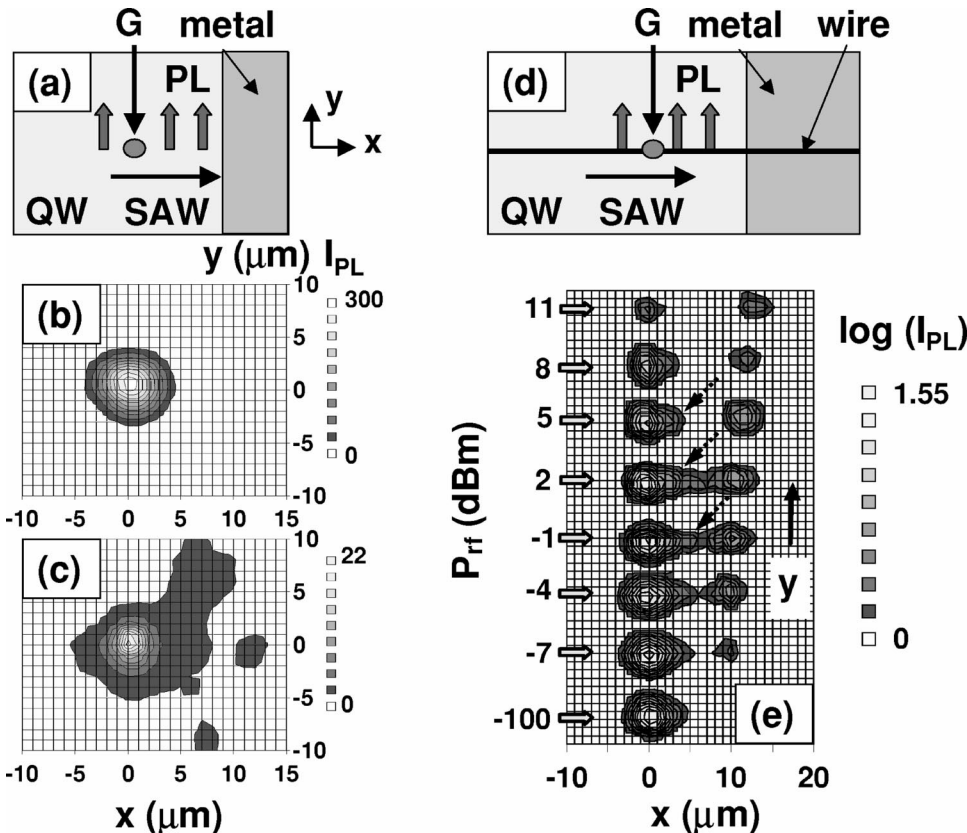


FIG. 3. Setup for spatially resolved PL measurements on (a) QW's and (d) QWR's. Spatial dependence of the QW PL generated by a microscopic laser spot (b) in the absence and (c) in the presence of a SAW. Under the influence of a SAW, the photogenerated carriers are transported along the SAW propagation direction until they recombine close to a metal stripe used to short circuit the piezoelectric field. (e) Ambipolar transport along a GaAs QWR for different SAW intensities specified in terms of the rf power P_{rf} applied to the acoustic transducer. The dashed arrows in (e) indicate recombination sites.

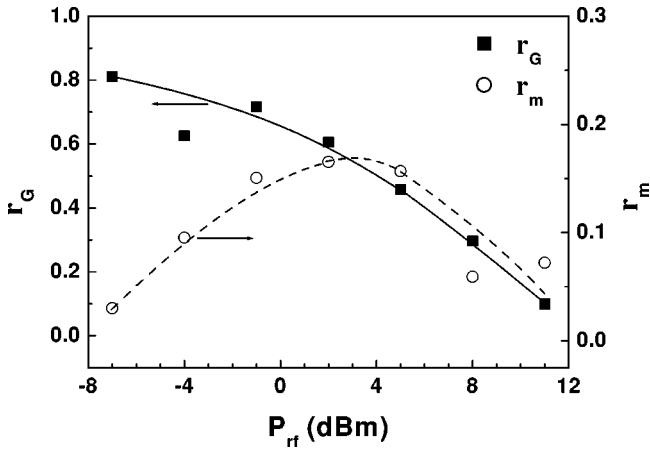


FIG. 4. Integrated PL intensity at the generation position (r_G , squares) and near the metal stripe (r_m , circles) as a function of the rf power applied to the IDT. r_G and r_m are normalized to the total PL intensity in the absence of a SAW. The lines are a guide to the eyes.

absence of a SAW, the PL intensity decays exponentially from G with a decay length corresponding to the characteristic exciton diffusion length in the QW.⁸ Under a SAW, the carriers are transported along the SAW propagation direction and recombine near the metal stripe. The increased recombination lifetime and, thus, diffusion length in the direction parallel to the wave fronts expands the recombination region along the y -direction.

The recombination area is markedly inhomogeneous in the presence of a SAW. The inhomogeneity is probably due to a distribution of defects in the QW, such as those reported in Ref. 7. In addition, the transport distances in the (311) QW's are much shorter than those reported in Ref. 7. This is at least in part associated with the smaller width of the QW used in the present studies, which increases the influence of the interfaces on the transport properties.

Similar results for carrier transport along QWR's [cf. Fig. 3(d)] are illustrated in Fig. 3(e), which shows PL (x, y) spatial profiles for different values of P_{rf} . The extent of the PL profiles along the y direction is determined by the experimental spatial resolution. As the SAW amplitude increases, carriers are transported along the QWR from the generation spot to the metal stripe. In contrast to the QW results, diffusion along the y direction is inhibited by the lateral barriers of the QWR. As a result, the carriers are transported as well-defined charge packages over large distances along the x -direction.

The squares and circles in Fig. 4 show the dependence of the integrated PL intensity at the generation position (r_G) and close to the metal stripe (r_m), as a function of P_{rf} . r_G and r_m are normalized to the integrated PL intensity in the absence of a SAW. They are associated with the PL quenching ratio and with the carrier transport efficiency from G to the metal edge, respectively. While r_G decreases monotonically with SAW amplitude, r_m first increases up to a maximum value of about 20% for $P_{rf}=2$ dBm, and reduces thereafter. For high P_{rf} levels, the piezoelectric field in the QWR under the metal region overcomes the value necessary

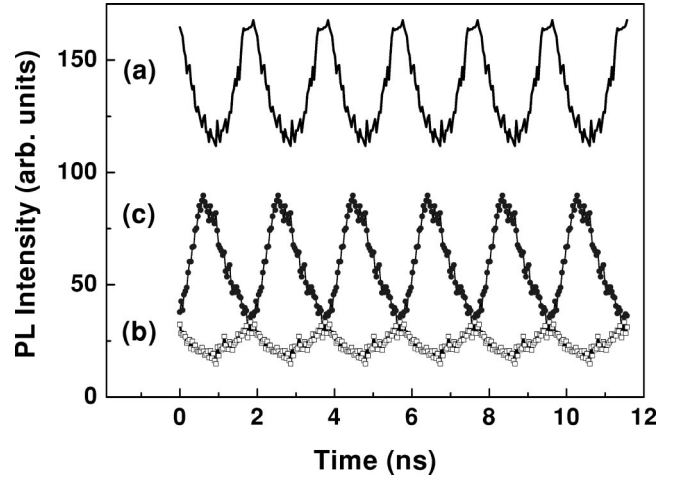


FIG. 5. Time-resolved PL for (a) and (b) coincident and (c) spatially separated excitation and detection areas, measured in the configuration of Fig. 3(d). SAW intensities were (a) $P_{rf}=21$ dBm and (b) and (c) $P_{rf}=23$ dBm. Continuous carrier generation was provided by cw illumination.

for ambipolar carrier transport under the metal, thus leading to a reduced carrier recombination probability close to the metal stripe. This effect becomes also evident in the distortion of the PL recombination profiles near the metal in Fig. 3(e) for $P_{rf} \geq 5$ dBm, where a spreading of the profiles along the SAW propagation direction is observed.

The transport efficiency is further affected by potential fluctuations in the QWR, which may act as carrier traps and induce recombination. In the PL profiles of Fig. 3(e), these potential inhomogeneities appear as bright recombination sites along the SAW propagation (see dashed arrows). The trapping and recombination probabilities reduce with the intensity of the SAW, as the piezoelectric potential becomes strong enough to overcome the barriers imposed by the fluctuations.

2. Carrier dynamics

In Sec. III C 1, the ambipolar transport of carriers by a SAW was investigated in the static limit. Further information about the transport dynamics is obtained from time-resolved experiments. Figures 5(a) and 5(b) show time-resolved PL traces measured for two different SAW amplitudes in the experimental configuration of Fig. 3(d). The measurements were performed using cw-laser excitation at a position G and by collecting the PL at the same position (confocal detection) using an APD. The PL detection energy was set at the maximum of the PL intensity. The SAW field modulates the PL signal at the fundamental frequency ω_{SAW} yielding pulses separated by the SAW period $T_{SAW}=1.9$ ns. The modulation is superimposed on a background, which becomes to a large extent suppressed as the SAW amplitude is increased [cf. Fig. 5(b)]. The suppression is related to an increase of the exciton ionization and the carrier transport efficiency with the magnitude of the piezoelectric field. The larger intensity of the trace in Fig. 5(c), which is recorded near the edge of the metal stripe (situated $8 \mu\text{m}$ away from

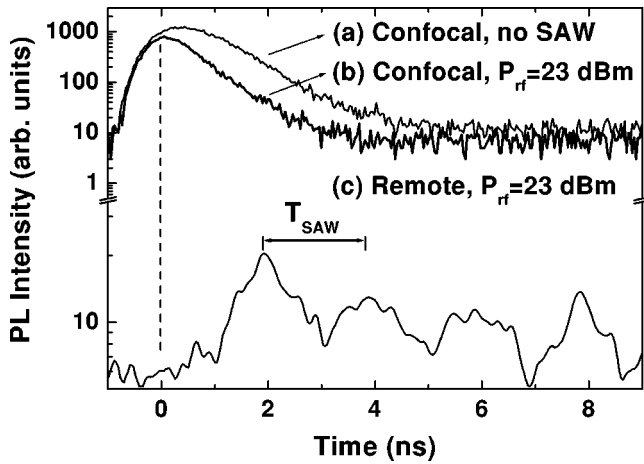


FIG. 6. Time-resolved PL recorded after pulsed illumination for (a) and (b) coincident and (c) spatially separated excitation and detection areas, measured in the configuration of Fig. 3(d).

the generation spot along the SAW propagation direction) supports this assertion. The relative phase between the traces for confocal and remote detection differs by 180° . The phase shift is associated with the distance between the generation and detection position of approximately $3\lambda_{\text{SAW}}/2$, which induces a delay of $3T_{\text{SAW}}/2$ for the SAW propagation time.

The time dependence of the PL emission is similar to that observed in QW structures.¹⁶ As in the QW case, it is attributed here to the dynamic distribution of the electron (n) and hole (p) densities in the SAW potential, which are controlled by the piezoelectric field and by the transport properties of the carriers. Due to the high mobility of the electrons, n is expected to peak at the maximum of the piezoelectric potential. In contrast, the lower mobility of the holes leads to a much wider distribution of p in the SAW potential. As a consequence, the recombination probability (proportional to the product np) peaks at the same position as the electron concentration n , i.e., the PL traces reflect the electron distribution in the piezoelectric potential.

Further evidence for the mechanism described in the previous paragraph is obtained from time-resolved measurements with pulsed illumination. Figures 6(a) and 6(b) display time-resolved PL traces measured in the confocal configuration after pulsed excitation in the absence and presence of a SAW, respectively. The rising time of the PL signal is determined by the finite resolution of the time-resolved setup. The reference time $t=0$ was calibrated by measuring the reflectance of the laser pulse used to excite the PL. Both PL traces in Figs. 6(a) and 6(b) show exponential decays with comparable decay times of 0.70 ns and 0.55 ns, respectively. As a consequence of the PL quenching, the trace in the presence of a SAW is narrower and has a lower peak amplitude.

In contrast to the PL detected at the generation spot, a PL trace recorded remotely at the edge of the metal stripe [Fig. 6(c)] shows a series of pulses with a repetition rate corresponding to the SAW period T_{SAW} . The delay of the arrival of the first pulse is related to the transport time of the carriers from the generation to the detection spot close to the metal.

The appearance of several PL pulses for a single generation pulse in Fig. 6(c) indicates that not all photogenerated carriers are transported within a single cycle of the SAW. A similar spreading of the detection time was observed recently by Rotter *et al.*¹⁷ during the unipolar transport of electrons by SAW's in two-dimensional electron gases for low SAW amplitudes. In the case of ambipolar transport investigated here, the presence of several pulses is attributed to the partial screening of the piezoelectric field by photogenerated carriers. The high carrier concentration created by the pulsed illumination partially screens the piezoelectric field near the generation spot. As a consequence, only a fraction of the carriers is transported in the first SAW cycle after the laser pulse. The remaining carriers are then transported during the subsequent SAW cycles, when the screening effect is reduced. The small degree of PL quenching under a SAW shown in Figs. 6(a) and 6(b) corroborates this statement. In addition, PL spectra recorded under the same excitation conditions show, instead of the characteristic sharp peaks in Fig. 2(a), a broad emission line, giving further evidence that a high-excitation power density is applied.

D. SAW-induced transfer between QW's and QWR's

1. Spatial profiles

The experimental configuration of Fig. 7(a), where the SAW propagates perpendicular to the QWR, allows for the study of the SAW-induced transfer of carriers from the QW to the QWR. The carriers, in this case, are generated by the microscopic spot G located in the QW several μm away from the QWR. The transfer process is illustrated in Figs. 7(b) and 7(c), which show the (x,y) dependence of the PL intensity integrated over the spectral emission regions of the QW and of the QWR, respectively. The QWR signal, which is only detected in the presence of a SAW, comes from carriers transported in the QW plane by the SAW potential and captured by the QWR confinement potential, where they recombine. The appearance of a weak signal at the QW position in Fig. 7(c) is related to the unavoidable overlap between the QWR PL spectrum and the low energy tail of the QW PL spectrum. The apparent spreading of the PL in the QWR shown in Fig. 7(c) is due to the lateral diffusion of the carriers in the QW [see Fig. 3(c)] during the transport from the generation point to the QWR.

Previous PL investigations on sidewall QWR's (Refs. 3 and 4) have given evidence of the existence of potential barriers for the transfer of excitons generated in the embedding QW to the QWR. As a consequence, carrier diffusion into the QWR becomes suppressed at low temperatures (below 70 K). At higher temperatures, however, carriers can be thermally excited across the barrier and captured into the QWR. The results of the previous paragraphs show that the carriers can easily overcome these barriers at low temperatures when excited by the SAW fields.

The contour plots in Figs. 7(b) and 7(c) were recorded using a SAW amplitude ($P_{\text{rf}}=11$ dBm) which maximizes carrier transfer from the QW to the QWR. The dependence of the PL distribution on the SAW amplitude is illustrated in

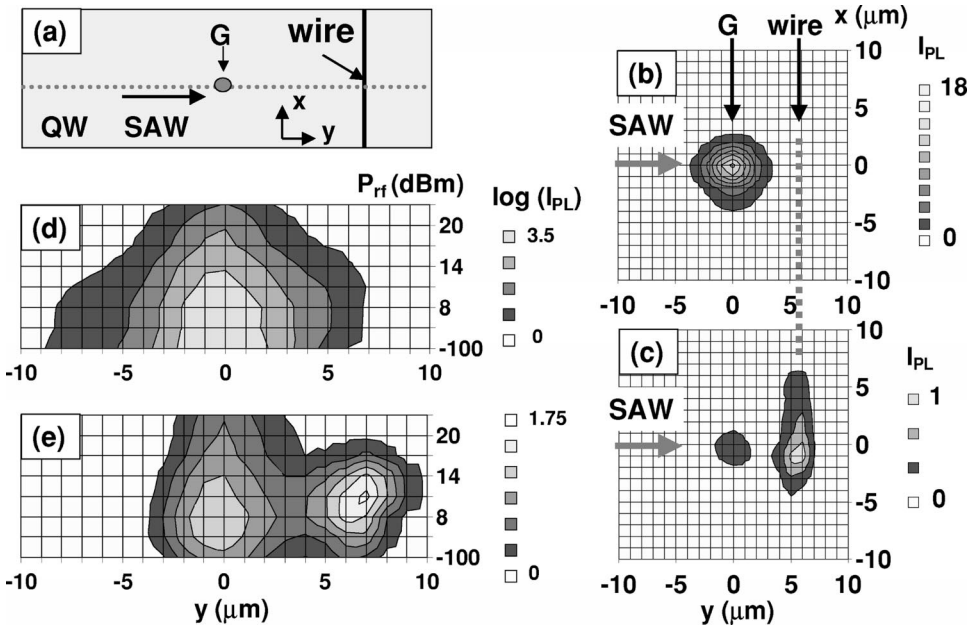


FIG. 7. (a) Experimental setup for carrier transport measurements from QW's to QWR's. The spatial distribution of the PL emission from the QW and for the QWR for a SAW amplitude $P_{rf}=11$ dBm are shown in (b) and (c), respectively. The contour plots in (d) and (e) show the PL intensity from the QW and QWR, respectively, as a function of the rf power (P_{rf} , vertical scale). The PL was excited at position G and detected along the dotted line in (a).

Figs. 7(d) and 7(e). The PL was detected along the y direction for different rf powers (vertical scale), and integrated over the energy range corresponding either to the QW [cf. Fig. 7(d)] or to the QWR signal [cf. Fig. 7(e)]. Up to rf powers of about 11 dBm, the PL intensity profiles from the QW show an abrupt reduction at the edge of the QWR ($y = 7 \mu\text{m}$). At this rf power level, the PL signal at the QWR position reaches its maximum intensity. Interestingly, a further increase of P_{rf} results in a decrease of the PL emission from the QWR.

The decrease and, eventually, the complete quenching of the QWR PL for high SAW intensities can be attributed to (i) an increase of the carrier diffusion length in the direction parallel to the wavefront, or (ii) to carrier extraction from the QWR potential by the SAW field. In order to check the first possibility, we measured the spatial dependence of the PL intensity along the QWR, i.e., parallel to the wavefront (not shown). The PL, in this case, was excited by a microscopic spot placed on the QWR position. While the carrier diffusion length along the QWR remains basically the same, the total integrated PL intensity shows a monotonic decrease with increasing P_{rf} . The lateral carrier diffusion is thus not the cause of the decay of the recombination rate.

The above results suggest that carriers can be extracted from the confinement potential of the QWR by the piezoelectric field, with an extraction probability increasing with the SAW intensity. The investigations mentioned above of Refs. 3 and 4 also demonstrated that at elevated temperatures carriers trapped in the sidewall QWR can be thermally excited into the the QW. In order to estimate if a similar process can be induced at low temperatures by a SAW, we determined the longitudinal electric field necessary to overcome the QWR confinement potential. For this purpose, we assumed as in Ref. 18 that the confinement energies for electrons and holes can be approximated as

$$U_i(y) = \varepsilon_i(0) + [\varepsilon_i(\infty) - \varepsilon_i(0)] \tanh^2(ay), \quad (1)$$

where $\varepsilon_i(0)$ and $\varepsilon_i(\infty)$ denote the energy in the wire ($y = 0$) and in the well ($y \rightarrow \infty$) for electrons ($i = e$) and holes ($i = h$). These energies, which are determined by the corresponding confinement potential, were obtained by assuming that the total exciton confinement energy of approx. 40 meV is distributed in a ratio of 6:4 between the conduction and valence bands. The full width at half maximum of the potential [given by $2 \arctanh(0.5)/a$] was taken equal to the QWR width of approximately 50 nm. The electric field necessary to completely flatten the confinement potential for electrons is found by deriving Eq. (1) to be approx. 3.4 kV/cm. This field corresponds to the longitudinal piezoelectric field of a $[\bar{2}33]/(311)$ SAW with an acoustic power density of about 30 W/m. By taking into account that the rf coupling losses are typically on the order of 7 dBm, we need a nominal rf power on the transducers of 13 dBm to generate such a SAW. This power level is consistent with the P_{rf} values in Fig. 7(e).

The process of carrier capture into and escape from the QWR is illustrated in Fig. 8. When the SAW potential energy $-q\Phi_{SAW}$ is minimum at the QWR position, electrons are transferred to the QWR [cf. Fig. 8(a)]. These negatively charged carriers can escape from the QWR potential when the SAW potential energy turns to zero and the induced longitudinal electric field reaches its maximal value [Fig. 8(b)]. Similar arguments can be used to describe the transfer and escape of holes during the second half of the SAW cycle [cf. Figs. 8(c) and 8(d)]. The behavior described above is expected to occur for large SAW amplitudes, where no carrier storage in the QWR takes place. For lower amplitudes, PL pulses are expected when electrons reach the QWR [as in Fig. 8(a)] and recombine with trapped holes.

We have tried to directly detect carriers extracted from the QWR by placing a metal stripe at the right side of the

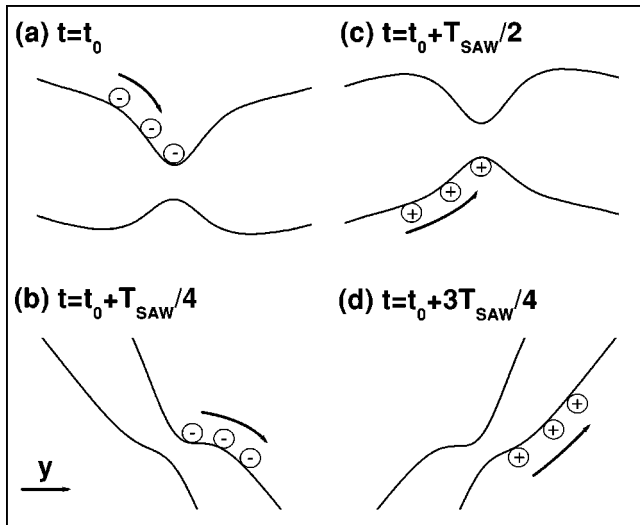


FIG. 8. Potential energy across the QWR as modified by the piezoelectric potential of a SAW for times corresponding to (a) minimum, (b) and (d) zero, and (c) maximum values of the potential energy of the SAW $-q\Phi_{\text{SAW}}$ at the QWR position.

QWR in Fig. 7(a) and by detecting at its edge the PL excited by a spot located at the QWR position. Unfortunately, the poor transport efficiency of the QW under study has prevented the detection of the weak PL signal in these experiments.

2. Carrier dynamics

The dynamics of the transfer process between QW's and QWR's is illustrated in Fig. 9(a), which shows the QWR PL in the experimental configuration of Fig. 7(a) after pulsed laser excitation. The remotely detected signal at the QWR position is characterized again by an oscillatory behavior with a pulse separation of T_{SAW} , i.e., carriers are periodically transferred to the QWR. As discussed above, this behavior is related to the high carrier concentration generated by the

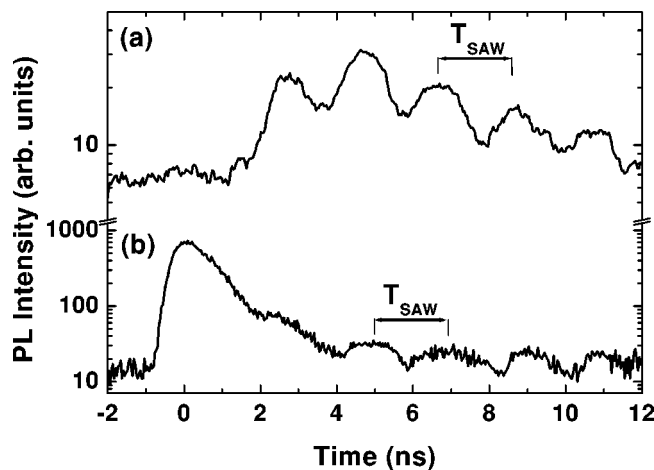


FIG. 9. Time-resolved PL recorded after pulsed illumination for (a) excitation in the QW and detection at the QWR areas and (b) coincident excitation and detection areas on top of the QWR.

pulsed laser. After a fraction of carriers is removed during the first SAW cycle, the reduction of the screening effect allows a more efficient transport in the second cycle. As a result, the intensity of the second pulse in Fig. 9(a) is higher than that of the first one.

For low SAW amplitudes, the time-resolved PL is expected to differ from the behavior of the previous paragraph because the carriers cannot leave the wire. Since the longitudinal piezoelectric field vanishes twice in a SAW cycle, it follows that the PL should be modulated at $2\omega_{\text{SAW}}$. In order to check this aspect, time-resolved measurements were performed with the generation spot placed directly on the QWR. The PL in this case [cf. Fig. 9(b)] shows a strong signal just after the pulsed laser excitation together with oscillations during the decay time. Contrary to the model discussed above, however, the oscillations have a period of T_{SAW} . The occurrence of a T_{SAW} period instead of the expected $T_{\text{SAW}}/2$ can be explained by the limited spatial resolution of our setup. The diameter of the laser spot is larger than the lateral dimensions of the QWR, so that carriers are also generated in the neighboring QW region. Therefore, we relate the oscillations in Fig. 9(b) to the transfer of these carriers to the QWR, which masks the observation of the carrier dynamics within the QWR.

The pulsed behavior described above was obtained in a regime of low and intermediate rf power P_{rf} , where QW-QWR carrier transfer processes dominate and the PL detected from the QWR shows oscillations at ω_{SAW} . For high P_{rf} , however, a suppression of the QWR confinement potential takes place and escape processes set in. In this case, the PL detected confocally from the QWR is strongly quenched and the pulsed behavior vanishes.

IV. CONCLUSIONS

We have investigated the ambipolar transport of photogenerated carriers between GaAs QW's and QWR's by the piezoelectric field of a SAW. The experiments were performed for SAW propagation parallel and perpendicular to the wires. In the first configuration, the confinement potential of the QWR prevents the lateral diffusion of the carriers, so that they are transported as well-defined charge packages over long distances along the wire. The transport mechanism is otherwise similar to that observed in QW's, with electrons and holes being transported at the maximum and minimum of the SAW potential, respectively. Potential fluctuations arising from inhomogeneities in the QWR thickness seem to be a source of carrier trapping, which undermine the transport efficiency. The trapping effect, however, can be overcome by increasing the SAW intensity. These results show that sidewall QWR's can be used as carrier transport channels without the deleterious surface recombination effects expected for etched channels.

The configuration where the SAW propagates perpendicularly to the QWR allows for a controlled transfer of carrier between the QW and QWR. We have observed two different

regimes in this configuration, which depend on the SAW amplitude. For low SAW intensities, transfer of carriers from the QW to the QWR has been proven to occur at the frequency of the SAW. For high SAW amplitudes, we give experimental evidence for the transfer of carriers trapped in the QWR into the QW. This occurs when the SAW piezoelectric field is sufficiently strong to overcome the QWR confinement potential.

ACKNOWLEDGMENTS

We thank H. Grahn and M. Ramsteiner for comments and for a critical reading of the manuscript. We acknowledge the technical expertise of S. Krauß in the preparation of the samples for the optical measurements. Support from the Deutsche Forschungsgemeinschaft (Project No. SA598/2-1) is gratefully acknowledged.

*Email address: falsina@pdi-berlin.de

- ¹Y. Arakawa and H. Sakaki, *Appl. Phys. Lett.* **40**, 939 (1982).
- ²R. Nötzel, M. Ramsteiner, J. Menninger, A. Trampert, H. P. Schönherr, L. Däweritz, and K. H. Ploog, *Jpn. J. Appl. Phys., Part 2* **35**, L297 (1996).
- ³A. Richter, G. Behme, M. Süptitz, Ch. Lienau, T. Elsaesser, M. Ramsteiner, R. Nötzel, K. H. Ploog, *Phys. Rev. Lett.* **79**, 2145 (1997).
- ⁴A. Richter, M. Süplitz, D. Heinrich, Ch. Lienau, T. Elsaesser, M. Ramsteiner, R. Nötzel, and K. H. Ploog, *Appl. Phys. Lett.* **73**, 2176 (1998).
- ⁵C. Rocke, S. Zimmermann, A. Wixforth, J. P. Kotthaus, G. Böhm, and G. Weimann, *Phys. Rev. Lett.* **78**, 4099 (1997).
- ⁶C. Bödefeld, A. Wixforth, J. Toivonen, M. Sopanen, and H. Lipsanen, *Phys. Status Solidi B* **224**, 703 (2001).
- ⁷S. K. Zhang, P. V. Santos, and R. Hey, *Appl. Phys. Lett.* **80**, 2320 (2002).
- ⁸T. Sogawa, P. V. Santos, S. K. Zhang, S. Eshlaghi, A. Wieck, and K. H. Ploog, *Phys. Rev. Lett.* **87**, 276601 (2001).
- ⁹R. Miskinis, P. Rutkowski, and E. Urba, *J. Appl. Phys.* **80**, 4867 (1996).
- ¹⁰V. Zhang, J.-E. Lefebvre, and T. Gryba, *IEEE Trans. Ultrason. Ferroelectr. Freq. Control* **44**, 406 (1997).
- ¹¹A. Crottini, J. L. Staehli, B. Deveaud, X.-L. Wang, and M. Ogura, *Phys. Rev. B* **63**, 121313(R) (2001).
- ¹²F. Intonti, V. Emiliani, Ch. Lienau, T. Elsaesser, R. Nötzel, and K. H. Ploog, *Phys. Rev. B* **63**, 075313 (2001).
- ¹³K. S. Zhuravlev, D. P. Petrov, Y. B. Bolkhovityanov, and N. S. Rudaja, *Appl. Phys. Lett.* **70**, 3389 (1997).
- ¹⁴P. V. Santos, M. Ramsteiner, and F. Jungnickel, *Appl. Phys. Lett.* **72**, 2099 (1998).
- ¹⁵T. Sogawa, P. V. Santos, S. K. Zhang, S. Eshlaghi, A. Wieck, and K. H. Ploog, *Phys. Rev. B* **63**, 121307(R) (2001).
- ¹⁶F. Alsina, P. V. Santos, R. Hey, A. García-Cristóbal, and A. Cantarero, *Phys. Rev. B* **64**, 041304(R) (2001).
- ¹⁷M. Rotter, A. V. Kalameitsev, A. O. Govorov, W. Ruile, and A. Wixforth, *Phys. Rev. Lett.* **82**, 2171 (1999).
- ¹⁸Ch. Lienau, A. Richter, G. Behme, M. Süptitz, D. Heinrich, T. Elsaesser, M. Ramsteiner, R. Nötzel, and K. H. Ploog, *Phys. Rev. B* **58**, 2045 (1998).